Biointerface Research in Applied Chemistry
Open-Access Journal (ISSN: 2069-5837)

Article
Volume 13, Issue 3, 2023, 217
https://doi.org/10.33263/BRIAC133.217

Designing of Novel Quinolines Derivatives as Hepatocellular Carcinoma Inhibitors by Using *In silico* Approaches

Reda El-Mernissi [1,*], Khalil El Khatabi [1], Ayoub Khaldan [1], Soukaina Bouamrane [1], Larbi El Mchichi [1], Mohammed Aziz Ajana [1,*], Tahar Lakhlifi [1], Mohammed Bouachrine [1,2]

[1] Molecular Chemistry and Natural Substances Laboratory, Faculty of Science, University Moulay Ismail, Meknes, Morocco; re.elmernissi@edu.umi.ac.ma (R.E.); khalil.elkhatabi@edu.umi.ac.ma (K.E.); ayoubkhaldan@gmail.com (A.K.); s.bouamrane@edu.umi.ac.ma (S.B.); elmchichi.larbi@gmail.com (E.L.); a.ajanamohammed@fs.umi.ac.ma (M.A.A.); tahar.lakhlifi@yahoo.fr (T.L.); bouachrine@gmail.com (M.B.)
[2] EST Khenifra, Sultan Moulay Sliman University, Beni mellal, Morocco; bouachrine@gmail.com (M.B.)
* Correspondence: a.ajanamohammed@fs.umi.ac.ma (M.A.A.);

Scopus Author ID 57216557017
Received: 5.03.2022; Accepted: 20.04.2022; Published: 5.06.2022

Abstract: Cancer is one of the very common diseases requiring long-term treatment, tubulin plays an important role in the development of cancer, and the use of colchicine binding site inhibitors against Hepatocellular Carcinoma has become the most common approach. A series of thirty quinoline derivatives have recently been identified as promising tubulin inhibitors with potent activity against human Hepatocellular Carcinoma. To design anti-cancer drugs, we applied the 3D-QSAR approach, this method is based on two contours (CoMFA and CoMSIA), the results obtained in two these contours are (R^2 = 0.98, Q^2 = 0.68, r^2ext = 0.96) and (R^2= 0.98, Q^2 = 0.57, r^2ext = 0. 97), respectively, this indicates that the model is trustworthy. The results indicate that the hydrophobic field contributes more (58%); based on these results, three quinoline derivatives (Z1, Z2, and Z3) are proposed as potent colchicine binding site inhibitors against hepatocellular carcinoma activities. Furthermore, molecular docking was utilized to compare the stability of complexes (ligand-receptor) based on the type of binding and the total score. The ADME has been utilized to evaluate the pharmacokinetic characteristics of the designed drugs; we can conclude that by using the results, all designed compounds are the best, and based on the results found at Docking and ADMET, and to identify the stability of newly compounds, molecular dynamic simulation was used for compounds Z2-3, the results found show that these molecules have better stability, which means that they have greater activity against hepatocellular carcinoma.

Keywords: quinolines; cancer; 3D-QSAR; molecular docking; ADME; molecular dynamics simulation (MD).

1. Introduction

Cancer is defined as the uncontrolled proliferation and development of aberrant cells [1]; researchers have found 100 types of cancer that require urgent treatment and diagnosis [2]. One of these cancers is hepatocellular carcinoma (HCC); this disease will be a global problem in 2025, affecting one million people worldwide [3]; in 2021 several studies have been done on this type of cancer [4-6], and each study analyzes one or more of the sides linked to this problem [7-10], it is the third deadliest and is the sixth most diagnosed cancer (7th in women

and 5th in men) [11,12] and is considered a serious public health problem [13,14], according to statistics, more than 800,000 people worldwide are afflicted by this kind of cancer each year [15,16]. The causes of hepatocellular carcinoma are hepatitis C and B virus (HCV and HBV), diabetes, alcoholic and non-alcoholic fatty liver disease (AFLD and NAFLD), and obesity. Additionally, Food pollutants, different environmental toxins, smoking, and familial or hereditary characteristics are all variables that contribute to the disease's occurrence [17-19]. Hepatitis C and B viruses (HCV and HBV) have been related to HCC for 1,000 years and 33,600,000 years, respectively [20,21], and most cases of HCC are initiated by liver cirrhosis [22,23], chemical carcinogens, in addition to viruses, have a part in causing this illness [24]. The number of studies on the causes of this chronic disease is endless and uncountable. Hormonal therapy, radiotherapy, chemotherapy, and surgery are the most used approaches in cancer treatment [25].

Due to their critical functions in cell division [26], microtubules are intriguing targets for cancer therapy [27,28]. It is formed by α–β-tubulin [29], tubulin has a linkage which is colchicine [30], elimination of colchicine binding site inhibitor (CBSI) microtubule formation by eliminating the vital tubulin assembly process remains the most widely used method against cancer [31], Quinoline derivatives are chemicals that have antineoplastic[32], antibacterial [33,34] antimalarial [35], and they inhibit cancer cell growth in a variety of ways [36], there is several heterocyclic molecules have the anticancer biological activity such as neocryptolepine, indoloquinoline, isocryptolepine, carbocycle-fused quinoline [37-40], Continuing to offer new drugs using the QSAR method [41-47], and those with anticancer activities [48-50], a family of 30 quinolines as potent colchicine binding site inhibitors against hepatocellular carcinoma was used to perform a 3D-QSAR study [51]. New compounds have been designed with higher activities. Molecular docking was used to characterize the different types of interactions and provide a total score, and the swissadmet web server was used to calculate the pharmacokinetic properties (ADME) of the compounds and to see the stability of some complexes. The dynamical simulation MD was used.

2. Materials and Methods

2.1. Prepared database.

The quinolines compounds used in this investigation were discovered in the literature [51] and were used to build 3D-QSAR models, the biological activities of the quinolines compounds were represented as (IC50.uM) and varied from (1,89 to 32,91), and the pIC50 was calculated to use the formula (pIC50 = -logIC50). The database of thirty molecules consists of all six molecules (*) and twenty-four molecules (training. The structures of compounds, as well as their experimental activity levels, are shown in Table 1. Figure 1 depicts the chemical structures of the substances investigated.

2.2. Optimization and alignment.

The 3D chemical structures of all derivatives were optimized using the Sybyl X-2.0 software (Tripos Inc., St. Louis, USA) and then optimized using the Tripos standard force field with a convergence threshold of 0.01 kcal/mol [52]; the Powell technique was used to add Gasteiger-Hückel charges to the compounds [53]. The optimization of all the studied compounds was carried out using the DFT method (B3LYP/6.311 (d, p)), to reach the

equilibrium geometry of each [54]. Compounds were aligned using the alignment approach; this step is very important to building a 3D-QSAR model [55], with compound 21 acting as a template. The primary conformations were previously minimized structures. Figure 2 illustrates the stacked architectures of aligning molecules.

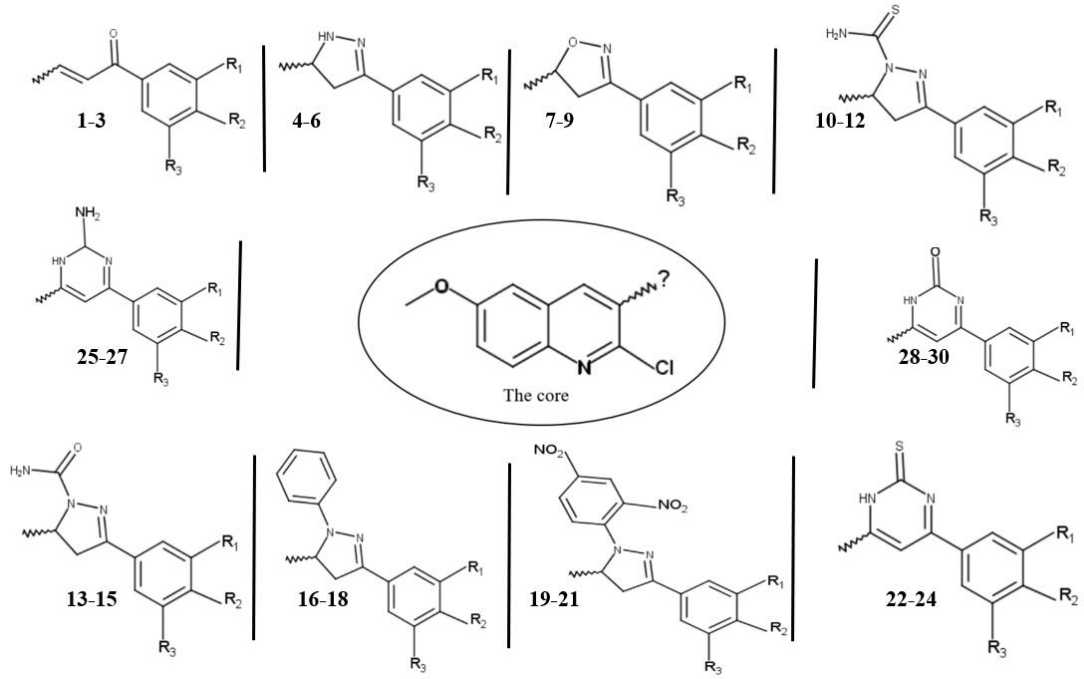

Figure 1. Structural template of studied compounds.

Table 1. pIC50 values of quinolines derivatives against Hepatocellular Carcinoma.

N°	R_1	R_2	R_3	pIC_{50}(M)	N°	R_1	R_2	R_3	pIC_{50} (M)
1	H	Cl	H	4.54	16	H	Cl	H	5.59
2	H	NH2	H	4.48	17	H	NH2	H	5.14
3	OCH3	OCH3	OCH3	4.63	18*	OCH3	OCH3	OCH3	5.32
4	H	Cl	H	4.51	19	H	Cl	H	5.58
5	H	NH2	H	4.78	20*	H	NH2	H	5.50
6	OCH3	OCH3	OCH3	4.81	21	OCH3	OCH3	OCH3	5.72
7	H	Cl	H	4.69	22	H	Cl	H	5.44
8	H	NH2	H	4.45	23*	H	NH2	H	4.79
9	OCH3	OCH3	OCH3	4.89	24	OCH3	OCH3	OCH3	5.26
10*	H	Cl	H	5.05	25	H	Cl	H	4.78
11	H	NH2	H	4.99	26	H	NH2	H	4.54
12	OCH3	OCH3	OCH3	5.03	27	OCH3	OCH3	OCH3	5.02
13*	H	Cl	H	4.90	28	H	Cl	H	5.09
14	H	NH2	H	4.99	29	H	NH2	H	5.03
15	OCH3	OCH3	OCH3	4.96	30*	OCH3	OCH3	OCH3	4.82

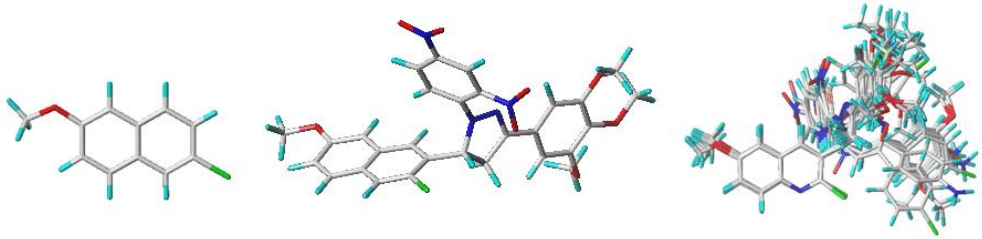

Figure 2. Core(left), 21 compound(middle), and alignment of compounds (Right).

2.3. Development of 3D-QSAR models.

The sybyl-x 2.0 program was used to examine the 3D-QSAR model. The two contours CoMFA and COMSIA were used to build this model and study the link with both the 3D structure and biological activity of these compounds [56,57]. The CoMFA contour increased

activity by using steric and electrostatic fields; in addition to these fields, the CoMSIA contour also exploited hydrogen bond acceptor (HBA), hydrogen bond donor (HBD), and hydrophobic characteristics of molecules. The column filtering value is set to 2.0 kcal/mol, and the energy cutoff is set to 30 kcal/mol, while the rest of the partial least square analysis (PLS) settings are launched by default [58].

High values of the coefficient of cross-validation correlation Q^2 and correlation coefficient R^2 ($Q^2 > 0.50$ and $R^2 > 0.60$) are two criteria to consider when picking a better model [59]. Other factors such as the optimal number of components (N), standard error of an estimate (SEE), and F-test value (F) are considered. The r^2ext parameter was also used to find the best predictive model based on a test set [60].

2.4. Molecular docking.

The first step in molecular docking is to download the protein tubulin (PDB ID: 1SA0) from the RSCB Protein Data Bank using the link (https://www.rcsb.org/); the RMSD between the co-crystal and redocked conformations of 1SA0 was less than 2 A°, indicating that the docking methodology used was reliable and may be used in future research. This active site of this protein has been chosen recently by several studies [61-63], then use the Surflex-Dock module in Sybyl 2.0, and finally use Pymol [64] and Discovery [65] software for preparation and to see the types of interactions.

2.5. ADMET prediction.

All medications influence the body bypass through the circulation, and to become effective drugs, they must pass through four stages: absorption, body distribution, metabolism, and excretion. These properties are abbreviated in the word ADMET; the swissadmet web server [66] was used to calculate these parameters for designed compounds (Z1 to Z3) and 21.

2.6. MD simulation.

The molecular docking was used to obtain the initial structures of the complexes to use for MD simulations. One of the ions (Na^+ or Cl^-) and the water molecule were added at a temperature of 300 K to obtain neutralization. The Desmond Dynamics software [67] obtains stability and conformational changes with time [68]. For the two proposed compounds, Z1 and Z2, the MD simulation duration was set to 50 ns for root-mean-square deviation (RMSD) and root-mean-square fluctuation (RMSF). To maintain the temperature and pressure, the Nose-Hoover system [69] and a Martyna-Tobias-Klein thermostat [70] were used.

3. Results and Discussion

3.1. 3D-QSAR analysis.

Internal and external validation was used to assess the accuracy of the 3D-QSAR model. The training set with N of 5 has an excellent non-cross-validated R^2 of 0.98 and a decent cross-validated Q^2 value of 0.68, according to the CoMFA contour, with an F-test of 186. 54, the lowest SEE is 0.034; these findings indicate that the model developed is satisfactory, the steric field-supplied 53 percent of the entire contribution, whereas the electrostatic field gave 47 percent of the total contribution in this model. The R^2 of the CoMSIA model was 0.98, with an optimum component of 4 and an acceptable Q^2 of 0.57. The resulting model exhibited a

high level of internal predictability, with a SEE value of 0.053 and an F-test score of 176.37. In this model, the proportions of steric, electrostatic, HBA, HBD, and hydrophobic sites were 11 percent, 10 percent, 13 percent, 8 percent, and 58 percent, respectively. The hydrophobic field was the most considered in the CoMSIA model when proposing novel anticancer compounds. For external validation, CoMFA and CoMSIA exhibited exceptional prediction capacity, and the external predictability of the two models, with r^2ext values of 0.96 and 0.97, respectively, further demonstrated the models' stability. Table 2 summarizes the statistical findings of the 3D-QSAR PLS study. Table 3 shows the observed and expected pIC50 of compounds. Figure 3 displays the dispersion of the observed and predicted pIC50 values and the correlation coefficient.

Table 2. PLS statistics parameters.

Model	Q^2	R^2	SCV	F	N	r^2_{ext}	Field Contribution (%)				
							Ster	Elec	HBA	HBD	Hyd
CoMFA	0.68	0.98	0.034	186.54	5	0.96	53	47	-	-	-
CoMSIA	0. 57	0.98	0.053	176.37	4	0.97	11	10	13	8	58

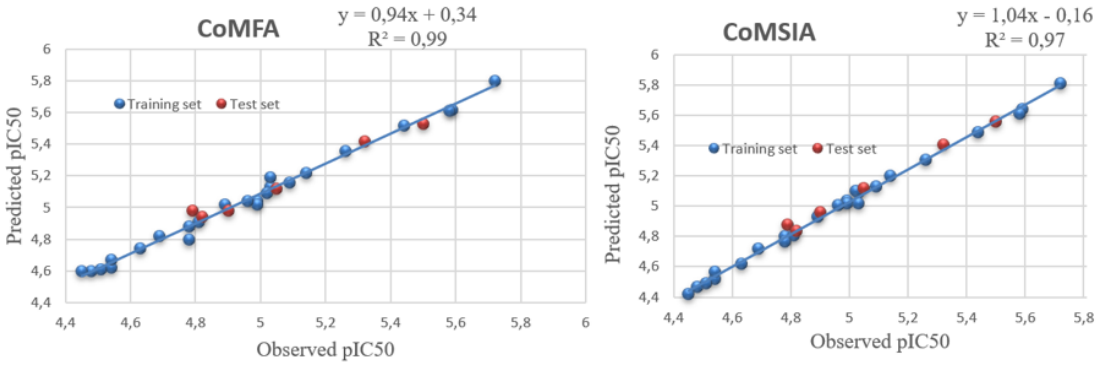

Figure 3. Plots of observed and predicted pIC50.

Table 3. Experimental and predicted activities of 30 novel quinolines derivatives.

N°	pIC50	CoMFA		CoMSIA	
		predicted	Residuals	predicted	Residuals
1	4.54	4.62	-0.08	4.52	0.02
2	4.48	4.60	-0.12	4.47	0.01
3	4.63	4.74	-0.11	4.62	0.01
4	4.51	4.61	-0.10	4.49	0.02
5	4.78	4.8	-0.02	4.8	-0.02
6	4.81	4.91	-0.10	4.81	0.00
7	4.69	4.82	-0.13	4.72	-0.03
8	4.45	4.60	-0.15	4.42	0.03
9	4.89	5.02	-0.13	4.93	-0.04
10*	5.05	5.12	-0.07	5.12	-0.07
11	4.99	5.04	-0.05	5.04	-0.05
12	5.03	5.13	-0.10	5.09	-0.06
13*	4.90	4.98	-0.08	4.96	-0.06
14	4.99	5.02	-0.03	5.02	-0.03
15	4.96	5.04	-0.08	5.01	-0.05
16	5.59	5.62	-0.03	5.64	-0.05
17	5.14	5.22	-0.08	5.20	-0.06
18*	5.32	5.42	-0.10	5.41	-0.09
19	5.58	5.61	-0.03	5.61	-0.03
20*	5.50	5.53	-0.03	5.56	-0.06
21	5.72	5.8	-0.08	5.81	-0.09
22	5.44	5.52	-0.08	5.49	-0.05
23*	4.79	4.98	-0.19	4.88	-0.09
24	5.26	5.36	-0.10	5.31	-0.05
25	4.78	4.88	-0.10	4.77	0.01

N°	pIC50	CoMFA		CoMSIA	
		predicted	Residuals	predicted	Residuals
26	4.54	4.67	-0.13	4.57	-0.03
27	5.02	5.09	-0.07	5.10	-0.08
28	5.09	5.16	-0.07	5.13	-0.04
29	5.03	5.19	-0.16	5.02	0.01
30*	4.82	4.94	-0.12	4.84	-0.02

The correlation coefficient and the dispersion of the points around the line show that our model was of good quality.

3.2. Contour maps analysis.

The most active compound 21, used as a reference in the CoMFA and CoMSIA contours, with default percentages of unfavored and preferred areas of 20% and 80%, respectively, was used to develop new compounds. The steric and electrostatic contours of the CoMFA field are presented in figure 4, while the Hydrophobic, HBD, and HBA contour maps of CoMSIA are revealed in Figure 5.

In figure 4 (a), the yellow colors represent that bulky groups are unfavored. The green colors represent that bulky groups are favored; this explains why compound 21 with a dinitro group has a maximum value of pIC50 (5.72) compared to other compounds. In figure 4 (b) the blue colors denote an unfavorable electronegative group, whereas the red colors denote an unfavorable electropositive group.

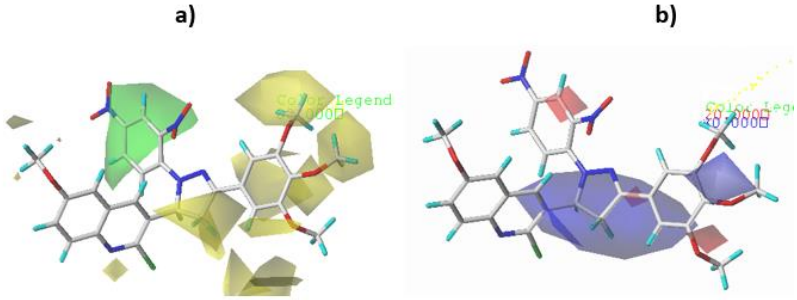

Figure 4. Contour maps of CoMFA analysis. a) Steric field; b) Electrostatic field.

The steric and electrostatic contours of CoMFA are identical to those of CoMSIA; and we do not discuss them. In Fig 5c, the hydrophobic field has a higher stake (58%) compared to other fields; as a result, we are unable to base our design on a hydrophobic field. Figure (5 c) shows the hydrophobic contour. The yellow and white colors represent that the added hydrophobic groups can increase and decrease activity. The 1,2,3trimethoxy substituents are covered by white color, indicating that adding hydrophobic groups decrease activity at these locations; this explains the order of activity of the experimental compounds, 5 > 4, 14 > 13. The yellow appears closer to one of the nitro and at closer positions; this was supported by the experimental activity identified in the following compounds, 21 > 10.

In Fig 5d, a cyan contour covers the 4,5-dihydro-1H-pyrazole molecule at the center of the most active compound, indicating that an HBD at this position was an advantage of the activity. In contrast, a purple contour covers the 2,4-dinitrobenzene molecule, which belongs to the most active compound; this indicates that the group's HBA increases its activity. This explains why experimental chemical 21 has greater activity (pIC50 = 5.72) than all experimental compounds.

In Figure 5e, a magenta outline covers the half surface of the 4,5-dihydro-1H-pyrazole molecule. The center of the most active compound indicates that an HBA group at this position was an advantage of the activity, while the red outline appears next to the nitro group, which belongs to the 2,4-dinitrobenzene molecule, which belongs to the most active compound; this indicates that the HBD groups can increase the activity. This also explains why compound 21 remains the most active.

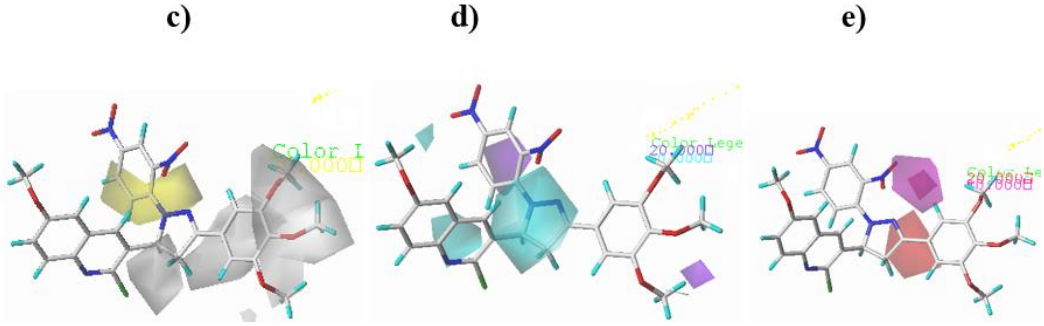

Figure 5. Contour maps of CoMSIA c) Hydrophobic field. d) HBD field. e) HBA field.

3.3. Design and prediction.

This article adds value to scientific research by proposing novel quinoline compounds as hepatocellular carcinoma inhibitors based on the 3D-QSAR model; this model was used to see the types of the most important fields to choose the substituents that can increase the activity of quinoline derivatives as inhibitors of hepatocellular carcinoma. As a result, three (Z1-Z3) novel quinoline compounds targeting tubulin were designed as hepatocellular carcinoma inhibitors; these compounds have a higher pIC50 than the most active (21) compound in the database, as shown in Table 4, which shows the structures of the proposed compounds as well as their calculated pIC50. According to the results of the total score, we can say that the stability of the complexes is classified in this order Z3> Z2>Z1>21.

Table 4. Newly designed compounds and their calculated pIC50.

N°	Compounds	Predicted pIC50	
		CoMFA	CoMSIA
21	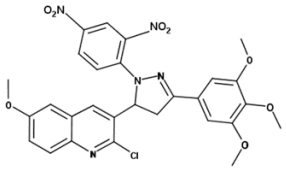	5.80	5.81
Z1	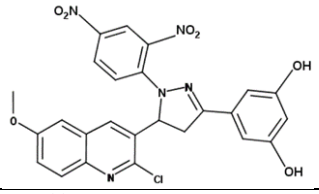	5.89	5.91
Z2	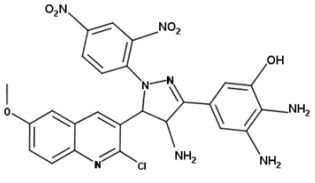	5.93	5.98
Z3		6.01	6.04

N°	Compounds	Predicted pIC50	
		CoMFA	CoMSIA
	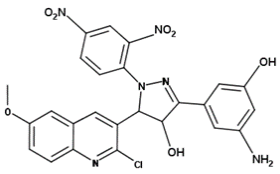		

3.4. Molecular docking.

The objectives of molecular docking in this part are to find the most stable complexes based on the interaction types listed in Table 5. All the compounds proposed have a conventional hydrogen bond interaction, except compound 21, which has none, increasing the stability of these compounds.

The 21 compound has three carbon hydrogen-bond(ALA 317, LYS 352, VAL 315), one of Halogen (Cl, Br, I) (ASN249), one of pi-sigma (LEU255), and five mixed Pi-Alkyl/Alkyl interactions(ALA 317-250,CYS 241,LEU 248,LYS 254).

Table 5. The interaction and total score.

N°	2D View	Total scoring	N°	2D View	Total scoring
21	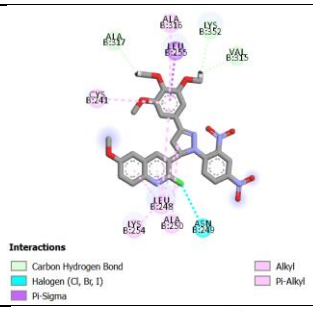	3.70	Z1	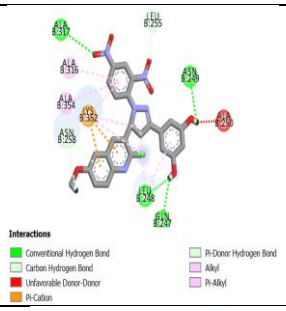	3.64
Z2	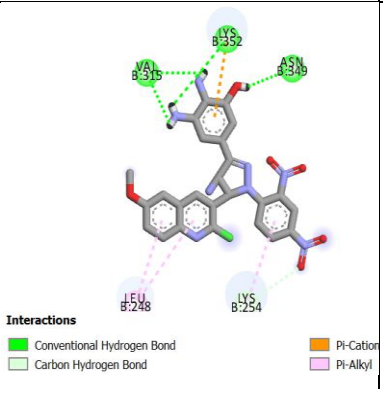	3.87	Z3	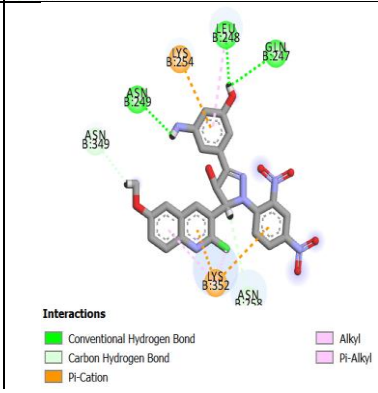	4.08

The first designed compound Z1 has several types of interaction, four conventional hydrogen Bond (ALA 317, ASN 249, LEU248, GIN247), one of the unfavorable donor-donor(ALA250), two mixed between Pi-Donor H-bond/Carbon H-bond (LEU255, ASN258), two mixed Pi-Alkyl/Alkyl (ALA316-354), and one of pi-cation type (LYS352) interactions. The existence unfavorable of interaction decreases the stability of this compound compared to the others proposed. While the second designed compound, Z2, has several types of interaction, three conventional hydrogen Bond (LYS 352, ASN 349, VAL 315), one of carbon H-bond (LYS 254), two of Pi-Alkyl (LEU 248, LYS 254), and one of pi-cation type (LYS 352) interactions. This molecule is stabilized by the presence of three conventional hydrogen bonds and the absence of any unfavorable interactions. The last compound proposed is Z3 has nine interactions of which, three conventional hydrogen bonds (ASN 249, LEU 248, GIN 247), two

carbon H-bond (ASN258, ASN349), two Pi-cation (LYS 352, LYS 254), and two interactions mixed between Pi-Alkyl/Alkyl (LYS 352, LEU 248).

The compound Z3 has the most favorable interactions, enhancing its stability, followed by compounds Z2 and Z1.

3.5. ADMET prediction.

The study of the active component of a medicine after it enters the body is known as pharmacokinetics, or "ADMET." It comprises four key steps: Absorption, Distribution, Metabolism, toxicity, and Excretion. The results of our compounds (21, Z1-Z3) are shown in table 6.

Table 6. ADMET prediction.

Model		**Compounds**			
		21	**Z1**	**Z2**	**Z3**
Absorption (A)					
Intestinal absorption (human)		90	100	84.22	93.865
Distribution (D)					
Blood-brain barrier (logBB)		-1.077	-1.735	-1.888	-1.632
Volume of distributionVDss (human)		0.14	0.18	0.21	0.41
Metabolism (M) : Yes (+), Non (-).					
Substrate (CYP)	2D6	-	-	-	-
	3A4	+	+	+	+
Inhibition (CYP)	1A2	-	-	-	-
	2C19	+	+	-	+
	2C9	+	+	-	+
	2D6	-	-	-	-
	3A4	+	+	+	+
Excretion (E)					
Clearence		0.49	0.52	0.60	0.70
Toxicity (AMES)		-	-	-	-

The first attribute is absorption, directly connected to the drug's absorption at the intestinal level (in humans). If the drug's absorption is less than 30%, it is deemed poorly absorbed by the body. All compounds have higher values that exceed the limit (>30%), but the proposed compound Z1 has higher values (100%).

The blood-brain barrier was identified in 1885 and has the primary purpose of isolating the central nervous system (CNS) from blood circulation; it prevents viruses, foreign chemicals, and potentially dangerous compounds from entering the brain and spinal cord. Compounds have a log BB value <-1; they cross the blood-brain barrier poorly; all compounds have respected this value; while the volume of distribution (VDss) is a second parameter characterizing the distribution of the active substance in the human body, the values are not accepted if (VDss)< -0.15 and are considered low, in the table above all the compounds designed to have a value of distribution not low.

Many medications can inhibit or increase the activity of a certain isoenzyme. More than one isoenzyme is involved in the metabolism of certain medicines. Approximately 90% of generally used medicines have four isoenzymes involved in their metabolism; the names CYP 1A2, CYP 2C9, CYP 2D6, and CYP 3A4 are used to describe these isoenzymes. The results show that all the compounds are inhibitors and substrates of CYP3A4; however, they are not inhibitors or substrates for CYP 2D6; in addition, only compounds 21, Z1, and Z3 are inhibitors of CYP C2C19 and C2C9.

Constant clearance describes the connection between drug concentration in the body and drug removal rate; when the clearance value is greater, the medication is deemed safe to

use; in the table above, the Z3 and Z2 compounds have a higher clearance value by Z1 compounds. Moreover, all molecules are not toxic.

We can conclude that all compounds are the best drug treatments for human hepatocellular carcinoma by using the results.

3.6. Molecular dynamics simulation (MD).

The docked conformers of compounds Z2 and Z3 have the highest hepatocellular carcinoma inhibitors activity of (pIC50= 5.93) and (pIC50= 6.01) were selected for molecular dynamics simulations (MD). Therefore, MD was performed for both ligand-protein complexes tubulin- Z3 and tubulin – Z2, the duration of the dynamic simulation was fixed at 50 ns, and results were analyzed by RMSD and RMSF. The graphs of RMSD, RMSF, and ligand-protein contacts diagrams of the two (tubulin-Z3, tubulin-Z2) complexes were illustrated in figures 6 (a, b, e, c, d, and f) successively.

In figure 4a, the RMSD of the designed molecule-protein complex Z3 deviated between 0 and 3.2 Å during the MD simulations; the RMSD is unstable between 0 and 20 ns then the RMSD of the ligand remains constant until 43 ns, then both RMSD (protein-ligand) remains confounded and remains stable to the rest of the simulation. In figure 4b, the RMSF values of the Z3 complex show that the maximum fluctuations are at residues 25,50,70,175,212,244,260,275,295, and 350, then with a maximum fluctuation of 4° at residue 420.

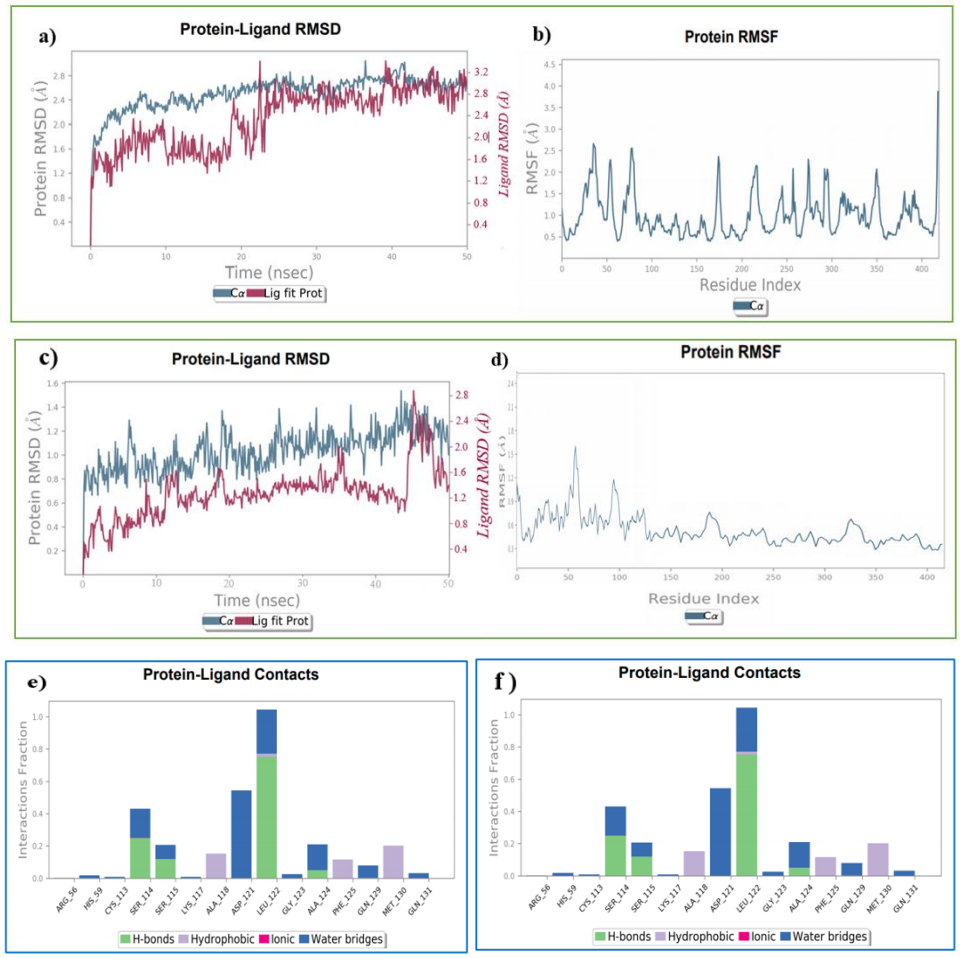

Figure 6. Root-mean-square deviation (a, c), root mean square fluctuations (b, d), and ligand-protein contacts diagrams.

The RMSD of the designed molecule-protein complex Z2 deviated between 0 and 2.8 Å during the MD simulations; the RMSD of protein and ligands has a value < 3 Å at 50 ns, showing the hence stability of this complex. In figure 4c, the RMSD is unstable between 0 and 18 ns, then the RMSD of the ligand remains constant until 45 ns, then both RMSD (protein-ligand) remain confounded and stable after this simulation. Figure 6d shows that the maximum fluctuations appeared at residues 60, 95, 190, and 340, reaching values 1,7 and 1,2, 0,8, and 0,8 A° successively. The rest of the residue has values between 0.3 and 0.7A°.

Hydrogen-bond, hydrophobic contact, ionic contacts, and water bridges were the four types of interactions studied. As seen in Figures 6(e and f), the findings were represented by stacked bar plots. The interaction diagrams clearly show that the two compounds Z2 and Z3 interact with the protein more positively.

4. Conclusions

Using *in silico* techniques, the 3D-QSAR model based on the CoMFA and CoMSIA contours was used to produce new quinoline derivatives as hepatocellular carcinoma inhibitors; the hydrophobic field is one of the fields used to select substituents that enhance the activity of compounds. Consequently, three novel tubulin inhibitors (Z1, Z2, and Z3) were designed, and to analyze the nature of the interaction between tubulin (receptor) and the designed molecule, the molecular docking showed that the compound Z3 has the best interactions, which improves its stability, followed by Z2 and lastly Z1; moreover, all compounds proposed have excellent pharmacokinetic characteristics (ADMET). The Molecular dynamic simulation showed that compounds Z3 and Z2 remained stable during the last 20 ns of the 50 ns. It's critical to synthesize these compounds, which might aid in developing tubulin polymerization inhibitors for the treatment of hepatocellular carcinoma.

Funding

This research received no external funding.

Acknowledgments

We are grateful to the "Association Marocaine des Chimistes Théoriciens" (AMCT) for its pertinent help concerning the programs.

Conflicts of Interest

The authors declare no conflict of interest.

References

1. Weinberg, R.A. How Cancer Arises. *Sci Am* **1996**, *275*, 62–70, https://doi.org/10.1038/scientificamerican0996-62.
2. Johnson, D.S.; Li, J.J. *The Art of Drug Synthesis*. Eds.; Wiley-Interscience: Hoboken, N.J, **2007**; https://doi.org/10.1002/9780470134979.
3. Philips, C.A.; Rajesh, S.; Nair, D.C.; Ahamed, R.; Abduljaleel, J.K.; Augustine, P. Hepatocellular Carcinoma in 2021: An Exhaustive Update. *Cureus* **2021**, *13*, https://doi.org/10.7759/cureus.19274.
4. Qing, X.; Xu, W.; Zong, J.; Du, X.; Peng, H.; Zhang, Y. Emerging Treatment Modalities for Systemic Therapy in Hepatocellular Carcinoma. *Biomarker Research* **2021**, *9*, https://doi.org/10.1186/s40364-021-00319-3.

5. Xu, G.; Jin, B.; Xian, X.; Yang, H.; Zhao, H.; Du, S.; Makuuchi, M.; Pawlik, T.M.; Mao, Y. Evolutions in the Management of Hepatocellular Carcinoma over Last 4 Decades: An Analysis from the 100 Most Influential Articles in the Field. *Liver Cancer* **2021**, *10*, 137-150, https://doi.org/10.1159/000513412.
6. Niu, M.; Yi, M.; Li, N.; Wu, K.; Wu, K. Advances of Targeted Therapy for Hepatocellular Carcinoma. *Frontiers in Oncology* **2021**, *11*, https://doi.org/10.3389%2Ffonc.2021.719896.
7. Muszbek, N.; Evans, R.; Remak, E.; Brennan, V.K.; Colaone, F.; Shergill, S.; Ross, P.; Mullan, D. Changes in Treatment Pattern and Costs in Advanced Hepatocellular Carcinoma (HCC). *Expert Review of Pharmacoeconomics & Outcomes Research* **2022**, *22*, 147–154, https://doi.org/10.1080/14737167.2021.1973892.
8. Lee, J.J.X.; Tai, D.W.-M.; Choo, S.P. Locoregional Therapy in Hepatocellular Carcinoma: When to Start and When to Stop and When to Revisit. *ESMO Open* **2021**, *6*, https://doi.org/10.1016/j.esmoop.2021.100129.
9. Lee, K.; Choi, G.H.; Jang, E.S.; Jeong, S.-H.; Kim, J.-W. A scoring system for predicting hepatocellular carcinoma risk in alcoholic cirrhosis. *Scientific Reports* **2022**, *12*, https://doi.org/10.1038/s41598-022-05196-w.
10. Song, J.; Zhou, H.; Gu, D.; Xu, Y. Hepatocellular Carcinoma Differentiation: Research Progress in Mechanism and Treatment. *Front Oncol* **2021**, *11*, https://doi.org/10.3389/fonc.2021.790358.
11. Ferlay, J.; Soerjomataram, I.; Dikshit, R.; Eser, S.; Mathers, C.; Rebelo, M.; Parkin, D.M.; Forman, D.; Bray, F. Cancer incidence and mortality worldwide: Sources, methods and major patterns in GLOBOCAN 2012. *International Journal of Cancer* **2015**, *136*, E359-E386, https://doi.org/10.1002/ijc.29210.
12. Ryerson, A.B.; Eheman, C.R.; Altekruse, S.F.; Ward, J.W.; Jemal, A.; Sherman, R.L.; Henley, S.J.; Holtzman, D.; Lake, A.; Noone, A.-M.; Anderson, R.N.; Ma, J.; Ly, K.N.; Cronin, K.A.; Penberthy, L.; Kohler, B.A. Annual Report to the Nation on the Status of Cancer, 1975-2012, featuring the increasing incidence of liver cancer. *Cancer* **2016**, *122*, 1312-1337, https://doi.org/10.1002/cncr.29936.
13. Cancer (IARC), T.I.A. for R. on. Global Cancer Observatory https://gco.iarc.fr/ (accessed 2022 -02 -11).
14. Villanueva, A. Hepatocellular Carcinoma. *N Engl J Med* **2019**, *380*, 1450–1462, https://doi.org/10.1056/NEJMra1713263.
15. Ferlay, J.; Colombet, M.; Soerjomataram, I.; Mathers, C.; Parkin, D.M.; Piñeros, M.; Znaor, A.; Bray, F. Estimating the global cancer incidence and mortality in 2018: GLOBOCAN sources and methods. *International Journal of Cancer* **2019**, *144*, 1941-1953, https://doi.org/10.1002/ijc.31937.
16. Thylur, R.P.; Roy, S.K.; Shrivastava, A.; LaVeist, T.A.; Shankar, S.; Srivastava, R.K. Assessment of risk factors, and racial and ethnic differences in hepatocellular carcinoma. *JGH Open* **2020**, *4*, 351-359, https://doi.org/10.1002/jgh3.12336.
17. Yang, J.D.; Hainaut, P.; Gores, G.J.; Amadou, A.; Plymoth, A.; Roberts, L.R. A global view of hepatocellular carcinoma: trends, risk, prevention and management. *Nature Reviews Gastroenterology & Hepatology* **2019**, *16*, 589-604, https://doi.org/10.1038/s41575-019-0186-y.
18. Sanyal, A.J.; Yoon, S.K.; Lencioni, R. The Etiology of Hepatocellular Carcinoma and Consequences for Treatment. *The Oncologist* **2010**, *15*, 14-22, https://doi.org/10.1634/theoncologist.2010-S4-14.
19. Jindal, A.; Thadi, A.; Shailubhai, K. Hepatocellular Carcinoma: Etiology and Current and Future Drugs. *Journal of Clinical and Experimental Hepatology* **2019**, *9*, 221-232, https://doi.org/10.1016/j.jceh.2019.01.004.
20. Paraskevis, D.; Magiorkinis, G.; Magiorkinis, E.; Ho, S.Y.W.; Belshaw, R.; Allain, J.-P.; Hatzakis, A. Dating the origin and dispersal of hepatitis B virus infection in humans and primates. *Hepatology* **2013**, *57*, 908-916, https://doi.org/10.1002/hep.26079.
21. Woolhouse, M.E.J.; Dye, C.; Simmonds, P. Reconstructing the origins of human hepatitis viruses. *Philosophical Transactions of the Royal Society of London. Series B: Biological Sciences* **2001**, *356*, 1013-1026, https://doi.org/10.1098/rstb.2001.0890.
22. Kanda, T.; Goto, T.; Hirotsu, Y.; Moriyama, M.; Omata, M. Molecular Mechanisms Driving Progression of Liver Cirrhosis towards Hepatocellular Carcinoma in Chronic Hepatitis B and C Infections: A Review. *International journal of molecular sciences* **2019**, *20*, https://doi.org/10.3390/ijms20061358.
23. Yang, J.D.; Kim, W.R.; Coelho, R.; Mettler, T.A.; Benson, J.T.; Sanderson, S.O.; Therneau, T.M.; Kim, B.; Roberts, L.R. Cirrhosis Is Present in Most Patients With Hepatitis B and Hepatocellular Carcinoma. *Clinical Gastroenterology and Hepatology* **2011**, *9*, 64-70, https://doi.org/10.1016/j.cgh.2010.08.019.
24. Desai, A.; Sandhu, S.; Lai, J.-P.; Sandhu, D.S. Hepatocellular Carcinoma in Non-Cirrhotic Liver: A Comprehensive Review. *World Journal of Hepatology* **2019**, *11*, 1–18, https://doi.org/10.4254/wjh.v11.i1.1.
25. Miller, K.D.; Siegel, R.L.; Lin, C.C.; Mariotto, A.B.; Kramer, J.L.; Rowland, J.H.; Stein, K.D.; Alteri, R.; Jemal, A. Cancer treatment and survivorship statistics, 2016. *CA: A Cancer Journal for Clinicians* **2016**, *66*, 271-289, https://doi.org/10.3322/caac.21349.
26. Chau, M.-F.; Radeke, M.J.; de Inés, C.; Barasoain, I.; Kohlstaedt, L.A.; Feinstein, S.C. The Microtubule-Associated Protein Tau Cross-Links to Two Distinct Sites on Each α and β Tubulin Monomer via Separate Domains. *Biochemistry* **1998**, *37*, 17692-17703, https://doi.org/10.1021/bi9812118.
27. Field, J.J.; Kanakkanthara, A.; Miller, J.H. Microtubule-targeting agents are clinically successful due to both mitotic and interphase impairment of microtubule function. *Bioorganic & Medicinal Chemistry* **2014**, *22*, 5050-5059, https://doi.org/10.1016/j.bmc.2014.02.035.

28. Kavallaris, M. Microtubules and resistance to tubulin-binding agents. *Nature Reviews Cancer* **2010**, *10*, 194-204, https://doi.org/10.1038/nrc2803.
29. Giannakakou, P.; Sackett, D.; Fojo, T. Tubulin/Microtubules: Still a Promising Target for New Chemotherapeutic Agents. *JNCI: Journal of the National Cancer Institute* **2000**, *92*, 182-183, https://doi.org/10.1093/jnci/92.3.182.
30. Botta, M.; Forli, S.; Magnani, M.; Manetti, F. Molecular Modeling Approaches to Study the Binding Mode on Tubulin of Microtubule Destabilizing and Stabilizing Agents. *Top Curr Chem* **2009**, *286*, 279–328, https://doi.org/10.1007/128_2008_20.
31. Lu, Y.; Chen, J.; Xiao, M.; Li, W.; Miller, D.D. An Overview of Tubulin Inhibitors That Interact with the Colchicine Binding Site. *Pharmaceutical Research* **2012**, *29*, 2943-2971, https://doi.org/10.1007/s11095-012-0828-z.
32. González-Sánchez, I.; Solano, J.D.; Loza-Mejía, M.A.; Olvera-Vázquez, S.; Rodríguez-Sotres, R.; Morán, J.; Lira-Rocha, A.; Cerbón, M.A. Antineoplastic activity of the thiazolo[5,4-b]quinoline derivative D3CLP in K-562 cells is mediated through effector caspases activation. *European Journal of Medicinal Chemistry* **2011**, *46*, 2102-2108, https://doi.org/10.1016/j.ejmech.2011.02.063.
33. Nandhakumar, R.; Suresh, T.; Jude, A.L.C.; Rajesh kannan, V.; Mohan, P.S. Synthesis, antimicrobial activities and cytogenetic studies of newer diazepino quinoline derivatives via Vilsmeier–Haack reaction. *European Journal of Medicinal Chemistry* **2007**, *42*, 1128-1136, https://doi.org/10.1016/j.ejmech.2007.01.004.
34. El Shehry, M.F.; Ghorab, M.M.; Abbas, S.Y.; Fayed, E.A.; Shedid, S.A.; Ammar, Y.A. Quinoline derivatives bearing pyrazole moiety: Synthesis and biological evaluation as possible antibacterial and antifungal agents. *European Journal of Medicinal Chemistry* **2018**, *143*, 1463-1473, https://doi.org/10.1016/j.ejmech.2017.10.046.
35. Mishra, M.; Mishra, V.K.; Kashaw, V.; Iyer, A.K.; Kashaw, S.K. Comprehensive review on various strategies for antimalarial drug discovery. *European Journal of Medicinal Chemistry* **2017**, *125*, 1300-1320, https://doi.org/10.1016/j.ejmech.2016.11.025.
36. Afzal, O.; Kumar, S.; Haider, M.R.; Ali, M.R.; Kumar, R.; Jaggi, M.; Bawa, S. A review on anticancer potential of bioactive heterocycle quinoline. *European Journal of Medicinal Chemistry* **2015**, *97*, 871-910, https://doi.org/10.1016/j.ejmech.2014.07.044.
37. El Sayed, I.E.; Ullah, S.; Al-Hartomy, O.A.; Hasanein, A.M.; Ahmed, A.A.S.; Kahilo, K.A.; El-Naggar, M.E. Synthesis, Nanoformulations, and In Vitro Anticancer Activity of N-Substituted Side Chain Neocryptolepine Scaffolds. *Molecules* **2022**, *27*, https://doi.org/10.3390/molecules27031024.
38. Vianney, Y.M.; Weisz, K. Indoloquinoline Ligands Favor Intercalation at Quadruplex-Duplex Interfaces. *Chemistry – A European Journal* **2022**, *28*, https://doi.org/10.1002/chem.202103718.
39. Nuthakki, V.K.; Mudududdla, R.; Bharate, S.B. Role of basic aminoalkyl chains in the lead optimization of Indoloquinoline alkaloids. *European Journal of Medicinal Chemistry* **2022**, *227*, https://doi.org/10.1016/j.ejmech.2021.113938.
40. Daoui, O.; Mkhayar, K.; Elkhatabi, S.; Chtita, S.; Zgou, H.; Elkhalabi, K. Design of Novel Carbocycle-Fused Quinoline Derivatives as Potential Inhibitors of Lymphoblastic Leukemia Cell Line MOLT-3 Using 2D-QSAR and ADME-Tox Studies. *RHAZES: Green and Applied Chemistry* **2022**, *14*, 36–61, https://doi.org/10.48419/IMIST.PRSM/rhazes-v14.31152.
41. Alaouy, M.A.E.; Youness, M.; Boutalaka, M.; Elbouhi, M.; Elmernissi, R.; Sbai, A.; Lakhlifi, T.; Bouachrine, M. The 2D-QSAR Study, Drug Likeness and in-Silico ADMET Prediction of about 3,5-Diaryl-1H-Pyrazole Derivatives as Multifunctional Agents for the Treatment of Alzheimer's Disease. *RHAZES Green Appl. Chem.* **2021**, *13*, 09–28, https://doi.org/10.48419/IMIST.PRSM/rhazes-v13.28095.
42. El Khatabi, K.; Aanouz, İ.; El-Mernissi, R.; Khaldan, A.; Ajana, M.A.; Bouachrine, M.; Lakhlifi, T. Designing of Novel Potential Inhibitors of A-Amylase by 3D-QSAR Modeling and Molecular Docking Studies. *J. Turk. Chem. Soc. Sect. Chem*. **2020**, 469–478, https://doi.org/10.18596/jotcsa.703026.
43. El Khatabi, K.; El-Mernissi, R.; Aanouz, I.; Ajana, M.A.; Lakhlifi, T.; Khan, A.; Wei, D.-Q.; Bouachrine, M. Identification of novel acetylcholinesterase inhibitors through 3D-QSAR, molecular docking, and molecular dynamics simulation targeting Alzheimer's disease. *Journal of Molecular Modeling* **2021**, *27*, https://doi.org/10.1007/s00894-021-04928-5.
44. Hajji, H.; En-nahli, F.; Aanouz, I.; Zaki, H.; Lakhlifi, T.; Ajana, M.A.; Bouachrine, M. Catastrophic Collision Between Obesity and COVID-19 Have Evoked the Computational Chemistry for Research in Silico Design of New CaMKKII Inhibitors Against Obesity by Using 3D-QSAR, Molecular Docking, and ADMET. *Orbital Electron. J. Chem*. **2021**, *13*, 316–327, https://doi.org/10.17807/orbital.v13i4.1608.
45. Khaldan, A.; Bouamrane, S.; El-Mernissi, R.; El Khatabi, K.; Aanouz, I.; Aggoram, A.; Sbai, A.; Bouachrine, M.; Lakhlifi, T. QSAR Study of α-Glucosidase Inhibitors for Benzimidazole Bearing Bis-Schiff Bases Using CoMFA, CoMSIA, and Molecular Docking. *Int. J. Quant. Struct.-Prop. Relatsh.* **2021**, *6*, 9–24, https://doi.org/10.4018/IJQSPR.2021010102.
46. El Khatabi, K.; Aanouz, I.; El-Mernissi, R.; Khaldan, A.; Ajana, M.; Bouachrine, M.; Lakhlifi, T. In Silico Analysis of 3D QSAR and Molecular Docking Studies to Discover New Thiadiazole-Thiazolone Derivatives

as Mitotic Kinesin Eg5 Inhibition. Moroc. *J. Chem.* **2021**, *9*, 9–405, https://doi.org/10.48317/IMIST.PRSM/morjchem-v9i2.18721.
47. Khaldan, A.; Bouamrane, S.; En-Nahli, F.; El-mernissi, R.; El khatabi, K.; Hmamouchi, R.; Maghat, H.; Ajana, M.A.; Sbai, A.; Bouachrine, M.; Lakhlifi, T. Prediction of potential inhibitors of SARS-CoV-2 using 3D-QSAR, molecular docking modeling and ADMET properties. *Heliyon* **2021**, *7*, https://doi.org/10.1016/j.heliyon.2021.e06603.
48. Elmchichi, L.; Belhassan, A.; Aouidate, A.; Ghaleb, A.; Lakhlifi, T.; Bouachrine, M. QSAR Study of New Compounds Based on 1,2,4-Triazole as Potential Anticancer Agents. *Physical Chemistry Research* **2020**, *8*, https://doi.org/10.22036/pcr.2019.204753.1685.
49. El-Mernissi, R.; El Khatabi, K.; Khaldan, A.; El Mchichi, L.; Ajana, M.A.; Lakhlifi, T.; Bouachrine, M. Design of new 3, 5-disubstituted indole as hematological anticancer agents using 3D-QSAR, molecular docking and drug-likeness studies. *Materials Today: Proceedings* **2021**, *45*, 7608-7614, https://doi.org/10.1016/j.matpr.2021.03.080.
50. El-Mernissi, R.; El Khatabi, K.; Khaldan, A.; ElMchichi, L.; Shahinozzaman, M.; Ajana, M.A.; Lakhlifi, T.; Bouachrine, M. 2-Oxoquinoline Arylaminothiazole Derivatives in Identifying Novel Potential Anticancer Agents by Applying 3D-QSAR, Docking, and Molecular Dynamics Simulation Studies. *J. Mex. Chem. Soc.* **2021**, *66*, https://doi.org/10.29356/jmcs.v66i1.1578.
51. Hagras, M.; El Deeb, M.A.; Elzahabi, H.S.A.; Elkaeed, E.B.; Mehany, A.B.M.; Eissa, I.H. Discovery of new quinolines as potent colchicine binding site inhibitors: design, synthesis, docking studies, and anti-proliferative evaluation. *Journal of Enzyme Inhibition and Medicinal Chemistry* **2021**, *36*, 640-658, https://doi.org/10.1080/14756366.2021.1883598.
52. Clark, M.; Cramer Iii, R.D.; Van Opdenbosch, N. Validation of the general purpose tripos 5.2 force field. *Journal of Computational Chemistry* **1989**, *10*, 982-1012, https://doi.org/10.1002/jcc.540100804.
53. Purcell, W.P.; Singer, J.A. A brief review and table of semiempirical parameters used in the Hueckel molecular orbital method. *Journal of Chemical & Engineering Data* **1967**, *12*, 235-246, https://doi.org/10.1021/je60033a020.
54. Lee, C.; Yang, W.; Parr, R.G. Development of the Colle-Salvetti Correlation-Energy Formula into a Functional of the Electron Density. *Phys. Rev. B* **1988**, *37*, 785–789, https://doi.org/10.1103/PhysRevB.37.785.
55. Khaldan, A.; Bouamrane, S.; El-Mernissi, R.; Maghat, H.; Ajana, A.; Sbai, A.; Bouachrine, M.; Lakhlifi, T. Identification of Potential α-Glucosidase Inhibitors: 3D-QSAR Modeling, Molecular Docking Approach. *Green and applied chemistry* **2021**, *12*.
56. Cramer, R.D.; Patterson, D.E.; Bunce, J.D. Comparative molecular field analysis (CoMFA). 1. Effect of shape on binding of steroids to carrier proteins. *Journal of the American Chemical Society* **1988**, *110*, 5959-5967, https://doi.org/10.1021/ja00226a005.
57. Klebe, G.; Abraham, U.; Mietzner, T. Molecular Similarity Indices in a Comparative Analysis (CoMSIA) of Drug Molecules to Correlate and Predict Their Biological Activity. *Journal of Medicinal Chemistry* **1994**, *37*, 4130-4146, https://doi.org/10.1021/jm00050a010.
58. Ståhle, L.; Wold, S. Chapter 6-Multivariate Data Analysis and Experimental Design in Biomedical Research. In: *Progress in Medicinal Chemistry*. Ellis, G.P.; West, G.B. Eds.; Elsevier, Volume 25, **1988**; pp. 291–338, https://doi.org/10.1016/S0079-6468(08)70281-9.
59. Golbraikh, A.; Tropsha, A. Beware of q2! *Journal of Molecular Graphics and Modelling* **2002**, *20*, 269-276, https://doi.org/10.1016/S1093-3263(01)00123-1.
60. Baroni, M.; Clementi, S.; Cruciani, G.; Costantino, G.; Riganelli, D.; Oberrauch, E. Predictive ability of regression models. Part II: Selection of the best predictive PLS model. *Journal of Chemometrics* **1992**, *6*, 347-356, https://doi.org/10.1002/cem.1180060605.
61. Elseginy, S.A.; Oliveira, A.S.F.; Shoemark, D.K.; Sessions, R.B. Identification and Validation of Novel Microtubule Suppressors with an Imidazopyridine Scaffold through Structure Based Virtual Screening and Docking. *bioRxiv* **2021**, https://doi.org/10.1101/2021.12.08.471724.
62. Daoui, O.; Mkhayar, K.; Khattabi, S.; Chtita, S.; Hsaine, Z.; Elkhalabi, R. Design of novel carbocycle-fused quinoline derivatives as potential inhibitors of lymphoblastic leukemia cell line MOLT-3 using 2D-QSAR and ADME-Tox studies. *RHAZES: Green and Applied Chemistry* **2022,** *14*, 36-61, https://doi.org/10.48419/IMIST.PRSM/rhazes-v14.31152.
63. Chalkha, M.; Akhazzane, M.; Moussaid, F.Z.; Daoui, O.; Nakkabi, A.; Bakhouch, M.; Chtita, S.; Elkhattabi, S.; Housseini, A.I.; El Yazidi, M. Design, synthesis, characterization, in vitro screening, molecular docking, 3D-QSAR, and ADME-Tox investigations of novel pyrazole derivatives as antimicrobial agents. *New Journal of Chemistry* **2022**, *46*, 2747-2760, https://doi.org/10.1039/D1NJ05621B.
64. DeLano, W. L. Pymol: An Open-Source Molecular Graphics Tool. CCP4 Newsl. *Protein Crystallogr*. **2002**, *40*, 82–92.
65. Dassault Systèmes BIOVIA, Discovery Studio Modeling Environment, Release 2017. San Diego: Dassault Systèmes. **2016**. Available online: https://www.3ds.com/products-services/biovia/products/molecular-modeling-simulation/biovia-discovery-studio/ (accessed February 6, 2020).

66. Daina, A.; Michielin, O.; Zoete, V. SwissADME: a free web tool to evaluate pharmacokinetics, drug-likeness and medicinal chemistry friendliness of small molecules. *Scientific Reports* **2017**, *7*, https://doi.org/10.1038/srep42717.
67. Robustelli, P.; Piana, S.; Shaw, D.E. Developing a molecular dynamics force field for both folded and disordered protein states. *Proceedings of the National Academy of Sciences of the United States of America* **2018**, *115*, E4758-e4766, https://doi.org/10.1073/pnas.1800690115.
68. Rinn, W.E. Emotional facial expression in Parkinson's disease: a response to Bowers (2006). *Journal of the International Neuropsychological Society* **2007**, *13*, 721-722, https://doi.org/10.1017/s1355617707070944.
69. Hoover, W.G. Canonical dynamics: Equilibrium phase-space distributions. *Physical Review A* **1985**, *31*, 1695-1697, https://doi.org/10.1103/PhysRevA.31.1695.
70. Martyna, G.J.; Tobias, D.J.; Klein, M.L. Constant Pressure Molecular Dynamics Algorithms. *J. Chem. Phys.* **1994**, *101*, 4177–4189, https://doi.org/10.1063/1.467468.